ACS Photonics

Article

pubs.acs.org/journal/apchd5

FRET from Multiple Pathways in Fluorophore-Labeled DNA

Joseph S. Melinger,*[,†] Ani Khachatrian,[‡] Mario G. Ancona,[†] Susan Buckhout-White,[§] Ellen R. Goldman,[§] Christopher M. Spillmann,[§] Igor L. Medintz,[§] and Paul D. Cunningham[†]

[†]Electronics Science and Technology Division, Code 6800, and [§]Center for BioMolecular Science and Engineering, Code 6900, U.S. Naval Research Laboratory, Washington, D.C. 20375, United States

[‡]Sotera Defense, 430 National Business Parkway, Suite 100, Annapolis Junction, Maryland 20701, United States

Supporting Information

ABSTRACT: Because of their ease of design and assembly, DNA scaffolds provide a valuable means for organizing fluorophores into complex light harvesting antennae. However, as the size and complexity of the DNA–fluorophore network grows, it can be difficult to fully understand energy transfer properties because of the large number of dipolar interactions between fluorophores. Here, we investigate simple DNA–fluorophore networks that represent elements of the more complex networks and provide insight into the Förster Resonance Energy Transfer (FRET) processes in the presence of multiple pathways. These FRET networks consist of up to two Cy3 donor fluorophores and two Cy3.5 acceptor fluorophores that are linked to a rigid dual-rail DNA scaffold with short interfluorophore separation corresponding to 10 DNA base pairs (~34 Å). This configuration results in five FRET pathways: four hetero-FRET and one homo-FRET pathway. The FRET properties are characterized using a combination of steady-state and time-resolved spectroscopy and understood using Förster theory. We show that the multiple FRET pathways lead to an increase in FRET efficiency, in part because homo-FRET between donor fluorophores provides access to parallel pathways to the acceptor and thereby compensates for low FRET efficiency channels caused by a static transition dipole distribution. More generally, the results show that multiple pathways may be used in the design of artificial light harvesting devices to compensate for inhomogeneities and nonideal ensemble effects that degrade FRET efficiency.

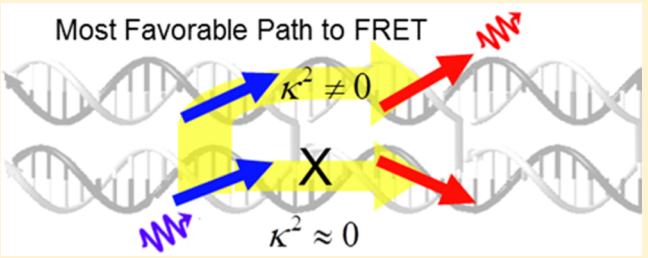

KEYWORDS: *Förster resonance energy transfer, FRET, DNA nanotechnology, light harvesting, photonic materials, photophysics*

DNA scaffolds provide a flexible means for organizing fluorophores into specific patterns to create useful functionality. The efficacy of the DNA scaffold derives from its ability to position fluorophores with a precision of down to 4 Å. Further, the ability to program DNA into complex three-dimensional shapes[1−4] allows the fluorophore network to be configured into virtually any three -dimensional arrangement. At a fundamental level, these capabilities allow new insight into the properties of Förster resonance energy transfer (FRET) in fluorophore networks.[5,6] At a more practical level the ability to tailor FRET in DNA–fluorophore structures suggests potential for photonics applications in molecular-based logic[7,8] and computing,[9] optical data storage,[10] chemical sensing,[11,12] biosensing,[13,14] light-harvesting,[5,15] and energy conversion devices.[16]

One challenge in the design of light harvesting materials is to gain control of the transition dipole orientations in order to optimize energy transfer efficiency. To date, there are only a few examples of control over fluorophore orientation in DNA structures, and these are restricted to relatively simple DNA structures.[17−19] In many cases, the DNA–fluorophore structures assemble with an unknown distribution of fluorophore orientations.[20,21] If the orientation distribution is static on the time scale of energy transfer, then the disorder can lead to degradation in the energy transfer efficiency because of the likelihood of transition dipole pairs assuming unfavorable orientations.[22] Thus, to create efficient synthetic light harvesting devices, it is important to consider design approaches that are robust to the effects of a nonideal assembly.

Recently, we showed that when fluorophores are arranged into networks that allow multiple FRET pathways to a terminal point then the energy transfer efficiency improves in comparison to networks that have only independent pathways.[5] Importantly, this strategy is biomimetic and is well-known to be exploited by photosynthetic systems.[23] Among artificial structures, this strategy has been nicely demonstrated in light harvesting dendrimers[24−26] and in other efficient light harvesting structures.[15] However, the photophysics in these structures can be difficult to understand because of the large number of fluorophore–fluorophore interactions. In this work we simplify the study of multiple energy transfer pathways by reducing the number of fluorophores to two donors and two acceptors, which allows us to separate the effects of homo-FRET (between like

Received: January 5, 2016
Published: February 24, 2016

DOI: 10.1021/acsphotonics.6b00006
ACS Photonics 2016, 3, 659−669

fluorophores) and hetero-FRET (between different fluorophores). We demonstrate experimentally that multiple FRET pathways significantly improve the FRET efficiency in the presence of a static distribution of fluorophore orientations. We theoretically confirm that homo-FRET gives access to alternative FRET pathways, increasing the likelihood of finding favorable transition dipole orientations. Our results provide a better understanding of how multiple FRET pathways compensate for FRET efficiency degradation caused by a static distribution and show that they may be used to mitigate nonideal ensemble effects in much larger self-assembled DNA-fluorophore networks.

MATERIALS AND METHODS

DNA Structure Assembly and Nomenclature. The overall DNA structure was designed from a DAE (double crossover alternating even)[27] based structure with two parallel template strands (DRtemp1 and 2) and a series of ∼1 helical turn staples of alternating 10 and 11 base pairs in length per side (DR1−5). The 5′ end of the tile has a 2 turn staple for stability. The de novo sequences were from Integrated DNA Technologies (Coralville, IA) with the exception of the Cy3.5-functionalized strands, which were purchased from Operon Biotechnologies, Inc. (Huntsville, Alabama). The sequences were selected such that each binding portion had no more than three complementary bases with the nondesired binding location, including self-complementarity and so that the melting temperature was significantly above room temperature (greater than 30 °C). The fluorophores were placed at the ends of the oligos, with either single 5′ labeling, or dual 5′ and 3′ labeling. For the Cy3 fluorophore, 5′ labeling presents a 3-carbon (3C) spacing from the end nucleotide and a 6-carbon (6C) space from the 3′ end of the final nucleotide. For the Cy3.5 binding, a 3C spacer exists between the dye and the end nucleotide for both the 3′ and 5′ ends. Both fluorophores are attached to the oligos using phosphoramidite chemistry. A schematic of the DNA structure (referred to in this work as the "dual rail") is shown in Figure 1a, and the DNA oligo sequences and chemical structures of the fluorophores are shown in Figure S1. The fully labeled dual rail contains two Cy3 donors and two Cy3.5 acceptors and is referred to below as **22** (Figure 1b). We also examine partially labeled rails of one donor and one acceptor (**11**), one donor and two acceptors (**12**), and two donors and one acceptor (**21**; Figure 1c). These variations allow us to separate the effects of homo-FRET and hetero-FRET interactions (Figure 1b). Finally, controls were included having only one (**1x**) or two (**2x**) Cy3 fluorophores or only one (**x1**) or two (**x2**) Cy3.5 fluorophores (Figure 1c).

Each DNA structure was self-assembled by one-pot hybridization of DNA oligos. Stock solutions of DNA were diluted into 2.5× phosphate buffered saline [PBS: 342.5 mM NaCl, 25 mM phosphate, 6.75 mM KCl; 2.5× PBS is obtained by dilution of a 10× PBS DNAase/RNAase-free stock purchased from Sigma-Aldrich (St Louis, MO)] at 20 μM working concentration. . Individual samples were assembled stepwise from component DNA (20 μM) in 0.5 mL of PCR or 1.5 mL microcentrifuge tubes to a final concentration of 1 μM in 2.5× PBS. Samples were vortexed repeatedly, microfuged, and then placed in a heating block with boiling water in the wells. The block was removed after 1 min, and the samples were allowed to cool to ambient temperature for 2 h, followed by brief microcentrifugation to collect the volume and 1 h incubation at 4 °C. A similar procedure was also used substituting a PCR thermal cycler for the heating block in which the temperature is held at 95° for 5 min and then ramped down at 1° per minute until 4 °C. Formation efficiency was assessed using a microfluidic automated electrophoresis system (Bio-Rad Experion) and was estimated to be between about 50−75% across all structures (Figure S2). To avoid degradation in yield, the samples were not purified after assembly, as in previous work.[5−7,28]

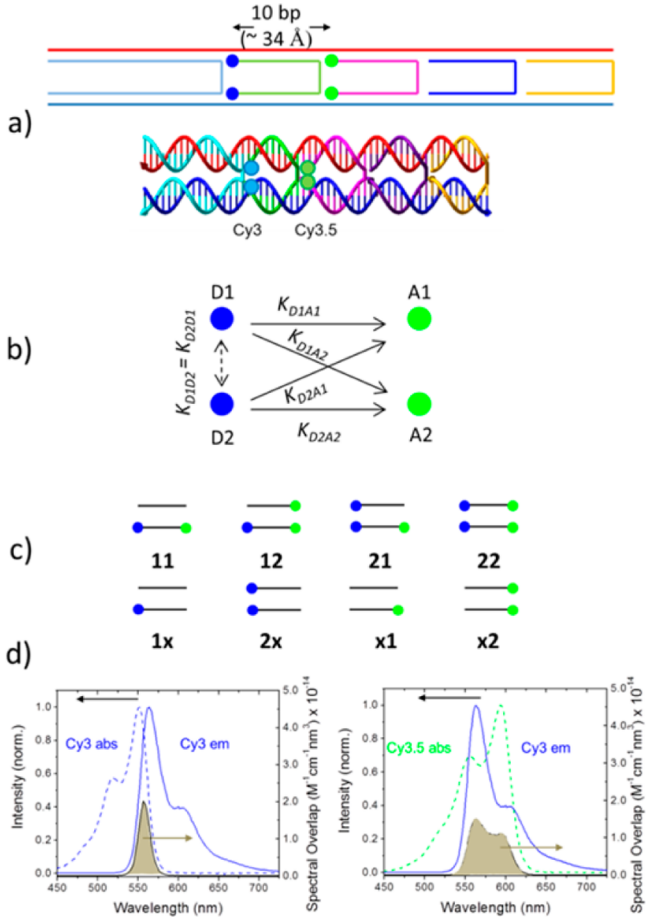

Figure 1. (a) Upper: Schematic of the dual rail DNA structure consisting of the self-assembly of seven DNA oligos, each depicted by a separate color. The Cy3 and Cy3.5 fluorophore positions at the ends of hairpin oligos are indicated by the solid blue circles and solid green circles, respectively. One of the Cy3 fluorophores is attached using a 3-carbon linker, while the other Cy3 is attached using a 6-carbon linker. The Cy3.5s are each attached using a 3-carbon linker. Lower: Schematic of the dual rail DNA structure showing the double crossover motif and positioning of the Cy3 and Cy3.5 fluorophores. (b) Schematic of the energy transfer pathways from Cy3 (solid blue circles) and Cy3.5 (solid green circles). The solid black arrows indicate hetero-FRET between a donor and acceptor and the dashed black double arrow is a homo-FRET coupling between the two donors. (c) Schematics of the FRET structures and control structures. (d) Normalized absorption and emission bands for the Cy3−Cy3 pair (left) and Cy3−Cy3.5 pair (right). The shaded gray areas indicate the spectral overlap function.

Spectroscopy and Procedures for Measuring FRET Efficiency. Steady state absorption spectra were measured using an Agilent 8453 diode array UV−vis spectrophotometer. Fluorescence spectra and fluorescence excitation profiles (FEP), corrected for instrumental effects, were measured on a Dual Monochromator Multifunction Microtiter Plate Reader (Tecan Safire). Since the flash lamp pulsewidth is much longer than the fluorescence lifetime, the measured spectra can be described as steady state spectra. All measurements were

DOI: 10.1021/acsphotonics.6b00006
ACS Photonics 2016, 3, 659−669

repeated for three independently made samples in 2.5× PBS buffer. Fluorescence quantum yields (QY) were measured using a Varian Eclipse spectrometer with a 90 deg excitation/detection geometry, and using samples with peak optical densities <0.1. The Cy3 fluorescence intensity was referenced to Rhodamine B in ethanol (QY = 0.68[29]), and the Cy3.5 fluorescence intensity was referenced to Sulforhodamine 101 in ethanol (QY = 0.9[30]). The Forster radii (R_0) were calculated from[31]

$$R_0 = 0.2108 \times (Q_D \times n^{-4} \times \kappa^2 \times J)^{1/6} \text{ Å} \quad (1)$$

where Q_D is the quantum yield of the donor (Cy3) in the absence of the acceptor, n is the refractive index taken to be 1.333 for water, κ^2 is the orientation factor for the absorption and emission transition dipoles, and J is the spectral overlap integral[31]

$$J = \int_0^\infty f_D(\lambda) \times \varepsilon(\lambda) \times \lambda^4 d\lambda \quad (2)$$

In eq 2, $f_D(\lambda)$ is the normalized fluorescence intensity of the donor in the absence of the acceptor and $\varepsilon(\lambda)$ is the molar absorptivity of the acceptor. The relevant quantities expressed in eqs 1 and 2 are collected in Table S1, which are then used to calculate the Förster radii for hetero-FRET and homo-FRET (also Table S1).

FRET quantum efficiencies were quantified through steady-state fluorescence measurements. FRET leads to simultaneous quenching of the donor emission and sensitization of the acceptor emission. For single donor, single acceptor cases, FRET efficiency is traditionally calculated by measuring donor loss or acceptor sensitization methods. For the multifluorophore labeled structures studied here (**12**, **21**, **22**), the fluorescence quenching of a donor pair and corresponding fluorescence sensitization of the acceptor pair were measured. In all experiments the excitation wavelength was 515 nm, which preferentially excited the Cy3 fluorophore. For the donor quenching method the FRET efficiency was estimated using the traditional donor quenching equation[31,32]

$$E_{DL} = 1 - \frac{F_{DA}}{F_D} \quad (3)$$

where F_{DA} represents the integrated fluorescence area of the donor in the presence of the acceptor, and F_D represents the integrated fluorescence area of the Cy3-only control structure. For example, to calculate the FRET efficiency of **21**, the integrated fluorescence area of 2Cy3 in the presence of Cy3.5 was referenced to the integrated fluorescence area of 2Cy3 in the absence of Cy3.5. When using the acceptor sensitization method, the FRET efficiency was estimated using the equation[32,33]

$$E_{sens} = \frac{F_{AD} - F_A}{Q_A} \Big/ \frac{F_D}{Q_D} \quad (4)$$

where F_{AD} is the integrated fluorescence area of the acceptor in the presence of the donor, F_A is the integrated fluorescence area of the acceptor in the absence of the donor, F_D is the integrated fluorescence area of the corresponding donor-only structure, and Q_A and Q_D are the fluorescence quantum yields of the acceptor and donor, respectively. For example, when using eq 4 to estimate the FRET efficiency for **22**, F_{AD} represents the integrated fluorescence area of the acceptor pair 2Cy3.5 when the donor pair 2Cy3 is excited. F_A represents the integrated fluorescence of the acceptor-pair 2Cy3.5 at the same excitation wavelength, and Q_A is for 2Cy3.5. F_D represents the integrated fluorescence area of the pair 2Cy3 at the same excitation wavelength, and Q_D is for 2Cy3. In all steady state measurements of donor loss or acceptor sensitization, the FRET samples and control samples were at equimolar DNA concentration. To recover F_{AD}, direct excitation of the acceptor and cross talk between the donor and acceptor were removed following the procedure given in ref 5. Briefly, first, the fluorescence spectrum of the acceptor (acceptors) at the excitation wavelength is recorded and subtracted from the donor−acceptor structure to remove the contribution of directly excited acceptor (acceptors). Next, single donor and acceptor spectra are scaled and added until they match the corrected donor−acceptor spectrum. This inherently corrects for overlap between donor and acceptor emission.

The Cy3 and Cy3.5 fluorescence lifetimes and FRET dynamics of the multifluorophore structures were measured via the time-correlated single photon counting (TCSPC) technique. The system was based on an 80 MHz, 7 ps pulsed, 532 nm, frequency-doubled, diode-pumped, Nd:YVO_4 laser (High-Q picoTRAIN). DNA duplexes in 2.5× PBS buffer solutions (~1 μM) were placed in a 1 mm path quartz spectrophotometric cell. The sample fluorescence was sent through a polarizer set to the magic angle[34] and then filtered using a monochromator. A micro channel plate photomultiplier tube (Hamamatsu) was used to detect the fluorescence. An instrument response function (IRF) with a full width at half-maximum (fwhm) of approximately 45 ps was measured using scattered light from a scattering solution in the fluorescence cell. The fluorescence decay dynamics of the donor(s) and rise time dynamics acceptor(s) were fit to a multiexponential function of three exponentials

$$A(t) = \sum_i A_i e^{-t/\tau_i} \quad (5)$$

where A_i and τ_i are the amplitude and the decay time, respectively, of the ith component of the function $A(t)$. The fitting was performed using the reconvolution software package Fluofit (Picoquant). The amplitude-average lifetimes were then calculated from[31]

$$\langle \tau \rangle = \sum_i A_i \tau_i / \sum_i A_i \quad (6)$$

The FRET efficiency was estimated from quenching of the donor time resolved signal using the formula[6,35]

$$E_{TR} = 1 - \frac{\langle \tau_{DA} \rangle}{\langle \tau_D \rangle} \quad (7)$$

where $\langle \tau_{DA} \rangle$ is the amplitude-average lifetime of the donor(s) in the presence of the acceptor(s) and $\langle \tau_D \rangle$ is the amplitude average lifetime of the donor(s)-only controls. As an example, when using eq 7 to calculate the FRET efficiency for **22**, $\langle \tau_{DA} \rangle$ represents the average lifetime of the Cy3 donor pair in the presence of Cy3.5 acceptor pair, and $\langle \tau_D \rangle$ represents the average lifetime of the Cy3 donor pair, **2x**. We emphasize that the use of three-exponentials is not motivated by requirements of FRET analysis. Instead, we find that three-exponential fits are required to adequately fit even single cyanine dye lifetimes. As such, all TCSPC decays are fit to three-exponentials and the dye lifetimes in both the absence and the presence of FRET are simply the weighted average of the time constants.

Time-resolved fluorescence anisotropy was determined by measuring the fluorescence decays for emission polarized parallel (I_{par}) and perpendicular (I_{per}) to the polarized excitation beam. The anisotropy was calculated from $r(t) = (I_{par} - GI_{per})/(I_{par} +$

DOI: 10.1021/acsphotonics.6b00006
ACS Photonics 2016, 3, 659−669

$2GI_{per}$). The quantity G (G-factor) is related to the different instrumental responses for parallel and perpendicular polarized emission.

Two-color pump−probe spectroscopy was also used to measure the FRET dynamics of the dual rail structures. The experimental setup was based upon a Ti:sapphire amplifier (CPA 2101, Clark-MXR), which was used to pump two optical parametric amplifiers (OPA). A noncollinear visible OPA was used to produce the pump pulse, while a frequency-doubled infrared OPA produced the probe pulse. Balanced Si photodiodes and a preamplifer were used to suppress noise. Lock-in detection of the ground-state bleach (GSB) or stimulated emission (SE) was used to measure the FRET dynamics, which are reported in terms of the delay-dependent normalized change in transmission ($\Delta T/T_0$). Preferential excitation of the Cy3 donor was maximized by tuning the pump pulse to 520 nm. The Cy3 donor decay dynamics were measured by tuning the probe pulse to 555 nm, and the Cy3.5 acceptor rise dynamics were measured by tuning the probe pulse to 605 nm. DNA duplexes in 2.5× PBS buffer solutions (∼1 μM) were placed in 1 cm path cuvettes, maintained at 10 °C using a cooling block connected to a water circulator, and stirred at 100 rpm throughout illumination to suppress photo or thermal degradation. The pump−probe IRF that was measured via two-photon absorption in ZnSe was 400 fs (fwhm), which is much faster than available through TCSPC. A 150 mm delay stage allowed for measurements up to a maximum pump−probe delay of 1 ns.

Modeling. The energy transfer dynamics as measured by ultrafast pump−probe spectroscopy was modeled using Monte Carlo simulation within the limit of Förster theory. Our approach is similar to the one used by Vogel et al.[22] who simulated FRET properties for a static isotropic distribution of fluorophore orientations. We have extended this approach to model donor decay and acceptor rise dynamics for a multifluorophore system. Details regarding the implementation of this model can be found in the Supporting Information.

RESULTS AND DISCUSSION

Figure 1a schematically shows the DNA scaffold consisting of two parallel and interconnected DNA double helices in a double crossover motif,[36] referred to here as a dual rail scaffold. The Cy3 and Cy3.5 fluorophores in these structures were separated by 10 base pairs, which correspond to a distance of approximately 34 Å. Because of the short linkers the distance between the Cy3 pairs and Cy3.5 pairs was also short and estimated to be ∼13 Å, based on a measurement of anisotropy resulting from homo-FRET (see below and SI). When fully labeled with two donors and two acceptors, the structure **22** exhibits five FRET interactions, four of which are hetero-FRET interactions between donor and acceptors, and one of which is a homo-FRET interaction between the two donors (Figure 1b). There is also a homo-FRET step that arises from the coupling between the two acceptors, however, this interaction is not relevant to the energy transfer from Cy3 to Cy3.5.

Figure 1d shows normalized absorption and fluorescence spectra for a Cy3−Cy3 homo-FRET pair and a Cy3−Cy3.5 hetero-FRET pair. The shaded areas show the spectral overlap functions (integrand of eq 2). The combination of large spectral overlap integrals (Table S1) and a relatively high fluorescence quantum yield for a single Cy3 fluorophore labeled on the DNA dual rail (**1x**: 0.37 ± 0.03) lead to favorable FRET properties for these fluorophore pairs. Within the dynamic isotropic limit,[21,22] the Förster radii (eq 1), $\hat{R}_0$, (where $\hat{R}_0$ is used to indicate R_0 for the special case of $\kappa^2 = 2/3$) are estimated to be 52 and 59 Å for the Cy3−Cy3 and the Cy3−Cy3.5 pairs, respectively.

1. Spectroscopy of Control Structures. Due to the relatively close spacing between the pair of Cy3s and the pair of Cy3.5s steady-state and time-dependent fluorescence measurements of the Cy3-only and Cy3.5-only controls were performed to check for potential strong electronic coupling effects. Comparison of absorption spectra and fluorescence excitation profiles (FEPs; Figure S3) were used as an initial indication of the strength of fluorophore−fluorophore coupling. With single fluorophore labeling, Cy3 (**1x**) and Cy3.5 (**x1**) have their respective absorption maxima at 555 and 596 nm. We note that the Cy3.5 peak absorption is red-shifted by about 10 nm from previous measurements.[5] The crowded microenvironment surrounding Cy3.5 likely restricts torsional motion about the methine bridge leading to a more planar molecule, thus red shifting the absorption spectrum. The addition of a second like fluorophore in the controls **2x** and **x2** finds similar absorption band shapes with the alterations in absorption position and band shape being small compared to the width of the absorption band. For **x2** the absorption shoulder near 550 nm is slightly pronounced with respect to the spectrum of **x1**, which suggests a small degree of aggregation for **x2**. Alterations of the blue side of the absorption spectrum is suggestive of H-type aggregation;[37] however, the effect here is quite small, indicating that only a small fraction of the ensemble for **x2** form such aggregates. The FEPs for **2x** and **x2** also generally match their respective absorption band shapes. Fluorescence quantum yield (QY) and fluorescence lifetime measurements provide a more sensitive measure of the electronic coupling between closely spaced fluorophores since the pairing of the fluorophores can result in some fluorescence quenching. For Cy3 the QY drops by 34%, going from 0.37 ± 0.03 for a single dye (**1x**) to 0.25 ± 0.02 for the pair (**2x**). Similarly, for Cy3.5 the QY drops by 28%, going from 0.42 ± 0.04 (**x1**) to 0.31 ± 0.04 (**x2**; Table S1). The fluorescence lifetimes shorten in a consistent manner when comparing measurements for **1x** and **2x**, and **x1** and **x2** (Figure S4 and Table S1). Taken together, these observations suggest that the paired Cy3-Cy3 and Cy3.5-Cy3.5 fluorophores are weakly coupled.

2. Restricted Fluorophore Motion. The rotational motions of the Cy3 and Cy3.5 attached to the DNA scaffold were investigated using time-resolved fluorescence anisotropy measurements of **1x** and **x1**, and the results are shown in Figure 2. For each structure, the decay in the anisotropy consisted primarily (∼89%) of a relatively slow relaxation (∼30 ns) and a minor (∼11%) fraction with a decay time of approximately 1 ns. The major fraction (slow component) in the anisotropy decay is associated with the tumbling motion of the DNA scaffold in solution,[35,38] and the minor fraction (∼1 ns decay) may be associated with restricted fluorophore motion in the DNA environment. This result indicates that the rotational motion of the Cy3 and Cy3.5 fluorophores is suppressed by the short linkers and the crowded environment of the surrounding DNA scaffold. As a comparison, the time-resolved anisotropy of free Cy3 has been measured and the anisotropy decays completely with a rapid 380 ps time constant, which is attributed to the rotational correlation time in solution.[39] Thus, the time-resolved anisotropy suggests that the transition dipole moments of the Cy3 and Cy3.5 fluorophores are relatively static on the time scale of energy transfer, as discussed in more detail below.

3. Energy Transfer Measurements of FRET Structures. The FRET efficiencies for **11**, **12**, **21**, and **22** were characterized

DOI: 10.1021/acsphotonics.6b00006
ACS Photonics 2016, 3, 659−669

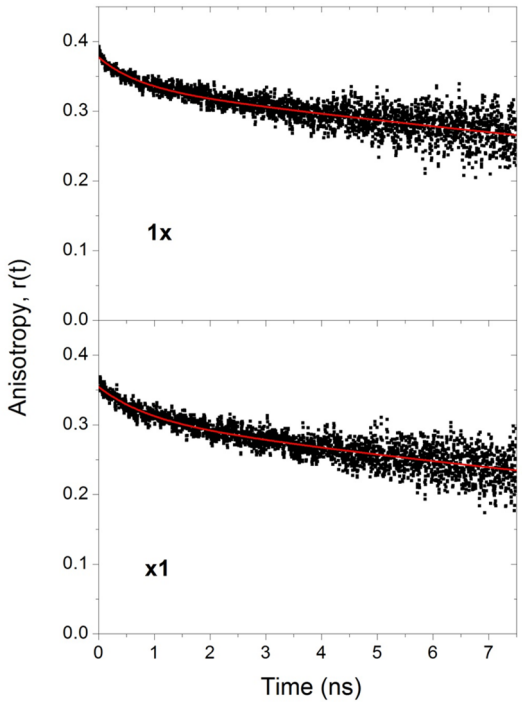

Figure 2. Time-resolved fluorescence anisotropy of dual rail control structures **1x** (top panel) and **x1** (bottom panel). The data in each panel represents the average of three measurements. The red lines are fits to the data using a biexponential decay function of the form $r(t) = a_1 e^{(-t/\tau_{r1})} + a_2 e^{(-t/\tau_{r2})}$, where τ_{r1} and τ_{r2} are interpreted as rotational correlation times. For the structure **1x**, the fitting yields $a_1 = 0.11$ and $\tau_1 = 0.8$ ns; $a_2 = 0.89$ and $\tau_2 = 32$ ns. For the structure **x1**, the fitting yields $a_1 = 0.11$ and $\tau_1 = 0.9$ ns; $a_2 = 0.89$ and $\tau_2 = 27$ ns. Here, the relative amplitudes of a_1 and a_2 are given in percent.

in three different ways based on their steady-state and time-dependent fluorescence with the results collected in Table 1. Shown in Figure 3 are examples of steady-state fluorescence spectra obtained by preferentially exciting the Cy3 donor at 515 nm and observing the quenched Cy3 emission (in comparison to the **1x** and **2x** controls at equimolar concentrations) and sensitized Cy3.5 emission due to FRET. The sensitized emission shown in Figure 3 is recovered after removing cross talk from Cy3 and direct excitation of Cy3.5.[5,28] As listed in Table 1, the FRET efficiencies estimated from the donor quenching (E_{DL}, eq 3) and from the acceptor sensitization (E_{sens}, eq 4) are similar in trend, though the E_{sens} are systematically lower by approximately 15−20 percentage points. The discrepancies in energy transfer efficiency, as measured by donor quenching and acceptor sensitization, which have been observed before,[20,32,40] suggest the presence of a nonradiative quenching mechanism so that not all of the quenched donor energy appears as acceptor fluorescence. One possible explanation for the discrepancy is an interaction between donors and acceptors in the excited state (or between an excited donor/acceptor and a nucleobase) through an electron transfer mechanism.[20] While such interactions would lead to lower FRET efficiencies for E_{sens} with respect to E_{DL}, our previous FRET studies of cyanine-labeled DNA[6] have not yielded evidence of photoinduced charge transfer bands, at least in the visible part of the spectrum. More work would have to be performed to rule out or substantiate a competing electron transfer mechanism. The third measure of efficiency (E_{TR}) comes from the time-resolved fluorescence measurements shown in Figure 4. The donor decays for each **11**, **12**, **21**, and **22** were nonexponential, which is a hallmark of inhomogeneity and consistent with a static isotropic dipole distribution. The corresponding acceptor inductions were difficult to observe due to spectral cross talk and direct excitation of the Cy3.5. To estimate energy transfer efficiency from the donor fluorescence decay curves they were fit to a sum of three exponentials and reconvolved with the instrument response function (eq 5 and Table S2) to determine an average lifetime (eq 6). The resulting energy transfer efficiencies (eq 7) are listed in Table 1. Each method of estimating FRET efficiency shows the same trend, such that the energy transfer efficiency increases in the order **11** < **21** < **12** < **22**. This is discussed further in the sections below.

Table 1. Energy Transfer Quantum Yields from Measurements and Theoretical Predictions

	experimental[a]			theory[e]
construct	E_{DL}[b]	E_{sens}[c]	E_{TR}[d]	E_{dyn}
11	0.70 (0.02)	0.52 (0.02)	0.60 (0.08)	0.96 [0.90]
21	0.73 (0.017)	0.57 (0.02)	0.70 (0.036)	0.96 [0.90]
12	0.80 (0.02)	0.61 (0.03)	0.76 (0.04)	0.98 [0.95]
22	0.83 (0.021)	0.65 (0.02)	0.84 (0.045)	0.98 [0.95]

[a]The numbers in parentheses indicate the standard deviation based on three independent measurements. [b]E_{DL} is the energy transfer efficiency measured by steady-state donor loss. [c]E_{sens} is the energy transfer efficiency measured by sensitization of Cy3.5 fluorescence. [d]E_{TR} is the energy transfer efficiency measured by time-resolved fluorescence (TCSPC) of the Cy3 donor. [e]E_{dyn}, calculated using the dynamic average limit $\kappa^2 = 2/3$ and $\frac{r}{\hat{R}_0} = 0.6$ based on r equal to a 10 bp separation (34 Å) between donor and acceptor. The values in brackets use $\frac{r}{\hat{R}_0} = 0.69$ based on $r = 41$ Å from the Monte Carlo modeling below.

4. Ultrafast Pump−Probe Measurements of FRET Structures. To complement the time-resolved fluorescence measurements, and to optimize the selective excitation/detection of Cy3/Cy3.5 kinetics, pump−probe spectroscopy was performed with tunable ultrashort (~150 fs) laser pulses. This permitted the observation of both the Cy3 donor decay dynamics and the Cy3.5 acceptor rise dynamics. To maximize selectivity, the pump pulse was tuned to excite the Cy3 band at 520 nm, and the probe pulse was tuned to 555 nm to monitor the Cy3 decay dynamics or to 605 nm (which corresponds to the peak of the transient absorption feature that combines the ground-state bleach and stimulated emission bands for Cy3.5) to measure the Cy3.5 induction dynamics. Plots of the normalized pump-induced change in sample transmission ($\Delta T/T$) for each construct are shown in Figure 5 (left panel). In each case, both a donor decay and acceptor rise are observed, confirming that the dynamics are due to FRET. Figure 5 also shows that both the donor decay dynamics and acceptor rise dynamics become faster in the order **11** < **21** < **12** < **22**, in agreement with E_{DL}, E_{sens}, and E_{TR}. We note the presence of a pedestal from which the Cy3.5 induction emerges. The origin of the pedestal is due in part to the direct excitation of Cy3.5, as well as to cross talk between the Cy3 and Cy3.5 responses. The solid lines in Figure 5 are results from a simulation model discussed below.

5. Theoretical Modeling. Many previous analyses of FRET in fluorophore-labeled DNA structures have assumed that the dynamic isotropic limit is valid, resulting in the orientation factor κ^2 set to 2/3 for each member of the ensemble. This presumes that the fluorophore transition dipoles are sufficiently dynamic to

DOI: 10.1021/acsphotonics.6b00006
ACS Photonics 2016, 3, 659−669

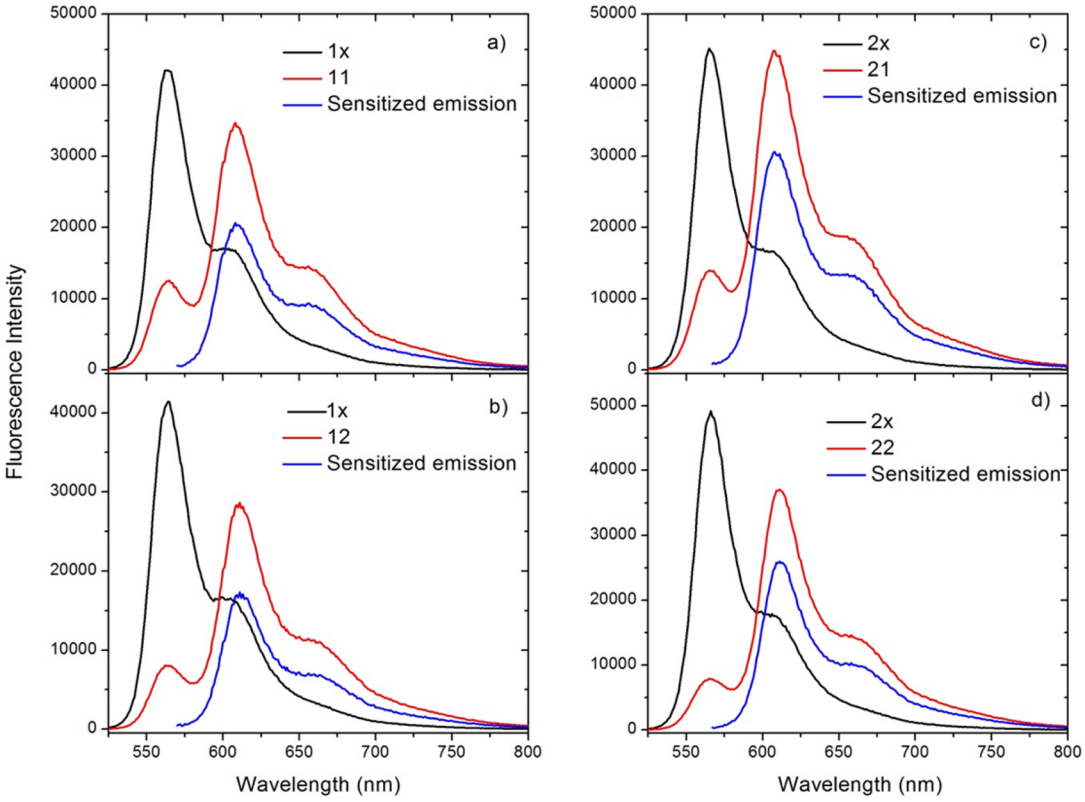

Figure 3. Steady state fluorescence spectra showing Cy3 donor loss and sensitized Cy3.5 fluorescence from dual rail structures. The black curves are the fluorescence spectra from Cy3-only controls and the red curves are fluorescence spectra from the Cy3−Cy3.5 dual rails. The blue curves represent the extracted sensitized Cy3.5 fluorescence after subtraction of direct excitation. Each panel represents a different target structure: (a) **11**, (b) **12**, (c) **21**, (d) **22**. In each case, the excitation wavelength is 515 nm.

sample a large number of orientations on the time scale of the FRET.[21,22] However, for our DNA structures, the dynamic isotropic limit does not appear to be valid, since our time-dependent fluorescence anisotropy measurements consisted mainly of relaxation on a time scale ∼30 ns that is slow compared to the FRET time scale (<500 ps). Providing further support for this conclusion is the fact that the dynamic $\hat{R}_0$ for the Cy3/Cy3.5 pair is approximately 59 Å, and with $\frac{r}{\hat{R}_0} \sim 0.6$, this implies an energy transfer efficiency of ∼96% for a single Cy3/Cy3.5 pair and ∼98% for a single Cy3 coupled to two Cy3.5s (both at the same separation from Cy3). But the energy transfer efficiencies derived from our steady-state and time-dependent spectroscopy (Table 1) were significantly below these values. Also, the addition of a second acceptor going from **11** to **12** produced a ∼18% relative increase in efficiency (averaging the increases from E_{DL}, E_{sens}, and E_{TR}), which is much higher than the ∼2% relative increase predicted by the dynamic isotropic limit. That the fluorescent donor decays were highly nonexponential also seems inconsistent with a uniform ensemble exhibiting dynamic averaging. The foregoing arguments indicate that our structures do not admit an assumption of dynamic dipole averaging on the FRET time scale, implying that their FRET properties cannot be understood on this basis. The observations summarized above suggest that the transition dipoles are quasi-static on the FRET time scale, thus, leading us to investigate whether the assumption of a static distribution of transition dipole orientations can give a better understanding. To this end, we assume the limiting case of an isotropic distribution of static transition dipole orientations. The orientation factor is defined as[41]

$$\kappa^2 = (3\cos^2(\theta) + 1)\cos^2(\omega) \tag{8}$$

where the angles θ and ω that define the relative transition dipole orientation are allowed to vary isotropically. As shown in ref 22, static isotropic dipoles produce a distribution (Figure S5) that is biased toward low values of κ^2, because there are more ways to produce unfavorable dipole orientations than favorable ones. To understand the effect this has on the FRET properties of our constructs, we perform Monte Carlo simulations based on Förster theory, in which each member of the ensemble, having a particular arrangement of dipole orientations determined at random, is evolved in time according to (for the case of **22**)

$$\begin{aligned}
\frac{dD_1^{(i)}(t)}{dt} &= -(K_D + K_{hom}^{(i)} + K_{D_1A_1}^{(i)} + K_{D_1A_2}^{(i)})D_1^{(i)}(t) \\
&\quad + K_{hom}^{(i)}D_2^{(i)}(t) \\
\frac{dD_2^{(i)}(t)}{dt} &= -(K_D + K_{hom}^{(i)} + K_{D_2A_1}^{(i)} + K_{D_2A_2}^{(i)})D_2^{(i)}(t) \\
&\quad + K_{hom}^{(i)}D_1^{(i)}(t) \\
\frac{dA_1^{(i)}(t)}{dt} &= -K_A A_1^{(i)}(t) + K_{D_1A_1}^{(i)}D_1^{(i)}(t) + K_{D_2A_1}D_2^{(i)}(t) \\
\frac{dA_2^{(i)}(t)}{dt} &= -K_A A_2^{(i)}(t) + K_{D_1A_2}^{(i)}D_1^{(i)}(t) + K_{D_2A_2}^{(i)}D_2^{(i)}(t)
\end{aligned} \tag{9}$$

DOI: 10.1021/acsphotonics.6b00006
ACS Photonics 2016, 3, 659−669

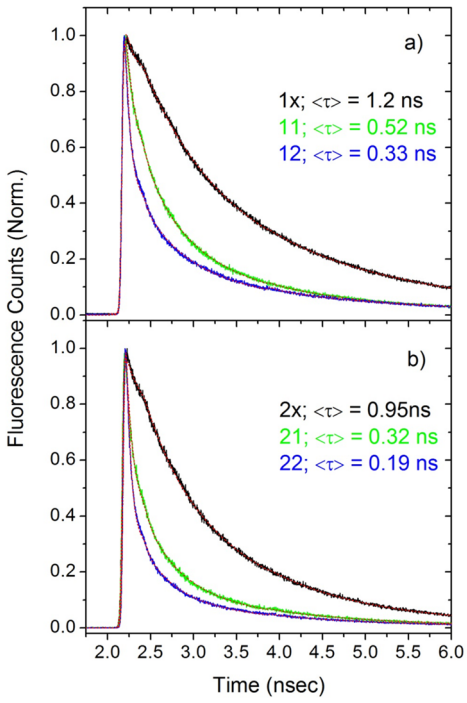

Figure 4. Comparison of time-dependent fluorescence curves for Cy3-only labeled dual rails and Cy3/Cy3.5 labeled dual rails: (a) **1x** (black curve), **11** (green curve), **12** (blue curve); (b) **2x** (black curve), **21** (green curve), **22** (blue curve). The red curves are fits to the data using a multiexponential decay function, as described in the text. For each construct, the average lifetime, τ_{av}, determined from the curve fitting procedure is given in the color-coded labels. The shoulders in each curve that appear near 2.5 ns are due to the instrument response of the detector.

where D_1, D_2, A_1, and A_2 represent the probabilities of the donor and acceptor fluorophores being excited, K_D and K_A are the excited state inverse lifetimes of the donor and acceptor fluorophores, $K_{hom} = K_{D_1D_2} = K_{D_2D_1}$ is the rate constant for homo-FRET between two donors, and $K_{D_jA_k}$ is the rate constant for hetero-FRET between the jth donor and the kth acceptor. The rate constants for hetero-FRET and homo-FRET are given by

$$K_{D_jA_k}^{(i)} = K_D\left(\frac{R_0^{(i)}}{r_{D_jA_k}}\right)^6$$

$$K_{hom}^{(i)} = K_D\left(\frac{R_0^{(i)}}{r_{D_1D_2}}\right)^6 \quad (10)$$

where $r_{DA}(r_{DD})$ is the donor−acceptor (donor−donor) distance, and $R_0^{(i)}$ is the Förster radius of the interaction. The distance $r_{D_1D_2}$ is estimated to be 13 Å based on a homo-FRET measurement using ultrafast pump−probe spectroscopy of the control **2x**, as described in the SI and in Figure S5. This corresponds to a transfer rate between Cy3 donors of ∼1 ps^{-1}, which is much faster than both the hetero-FRET rate (>1 ns^{-1}) and inverse excited state lifetime (∼1 ns^{-1}). Considering the placement of the Cy3 donors on the dual rail structure (Figure 1a and Figure S1), this estimate for the Cy3−Cy3 separation is reasonable. The homo-FRET coupling between the two acceptors has not been included because homo-FRET does not affect the excited state lifetime of the acceptor pair.[41] In eqs 9 and 10, the superscript i labels the member of the ensemble having a particular arrangement of orientations. Ensemble averaging the solutions to eq 9 one arrives at an estimate of the transient behavior that can be compared with the experimental data of Figure 5. One then looks to make physically plausible adjustments in the donor−acceptor distance in such a way as to fit the Cy3 decay dynamics and Cy3.5 induction dynamics for all constructs. The solid lines in Figure 5 represent the results of the Monte Carlo calculation and are found to reasonably simulate the experimental data using $D_1 \rightarrow A_1$ and $D_2 \rightarrow A_2$ distances of 41 Å, which is somewhat larger than the ∼34 Å separation corresponding to the 10 base pair separation between Cy3 and Cy3.5 fluorophores; this discrepancy may partially be due to the linker lengths (∼10 Å). The DNA structure can also assume slightly different configurations than predicted along with breathing dynamically,[5,28,42] all of which may alter separation distances.

Two aspects of our model need to be discussed. First is the treatment of the energy transfer using Förster theory. While the point dipole approximation (PDA) is reasonable for the hetero-FRET step with donor−acceptor distances of about 40 Å,[6,43,44] the PDA is questionable for the homo-FRET step where the donor−donor distances of about 13 Å are comparable to the size of the fluorophores. Presumably, a more accurate treatment of the energy transfer may be obtained by methods that consider the full Coulomb coupling between donor and acceptor.[44] As a test of the robustness of the model used here (eqs 9) to the homo-FRET step, we have performed simulations using larger $r_{D_1D_2}$ of up 20 Å while keeping r_{DA} fixed, which reduces the homo-FRET rate by 2 orders of magnitude. We found that the donor decay and acceptor induction dynamics show only small deviations and a corresponding small, 3%, change in FRET efficiency. This demonstrates that the hetero-FRET dynamics does not depend on the exact value of the homo-FRET rate, as long as the homo-FRET rate is significantly faster than the hetero-FRET rate. However, this simple picture would break down in the limit of strong donor−donor coupling such that the donors can no longer be thought of as independent. As pointed out above, the similarity of the absorption spectra and FEP for **1x** and **2x** suggest that the coupling of doubly labeled Cy3 donors is weak enough that they may be considered as independent donors.

Second, the model outlined above does not consider the effect of formation errors. The presence of partially formed structures containing incomplete fluorophore labeling can affect both the donor decay and acceptor rise dynamics. Formation efficiency can be used as a parameter in the model, however, without full knowledge of the types of formation errors (i.e., how much of each fluorophore is missing in a structure), it is difficult to quantitatively account for the contribution of partially formed structures. In previous work,[5] formation errors were used in modeling FRET spectra of multifluorophore DNA structures by introducing simplifying assumptions about the nature of the formation error. Here, we have chosen to assume complete formation in our model, using a single parameter, the donor−acceptor separation distance, to simulate the time-resolved FRET experiment.

As an aid to understanding how multiple pathways improve FRET efficiency, we gather statistics from the Monte Carlo simulations regarding the distribution of energy transfer efficiencies in the ensembles (Figure 5, right panel). In the

DOI: 10.1021/acsphotonics.6b00006
ACS Photonics 2016, 3, 659−669

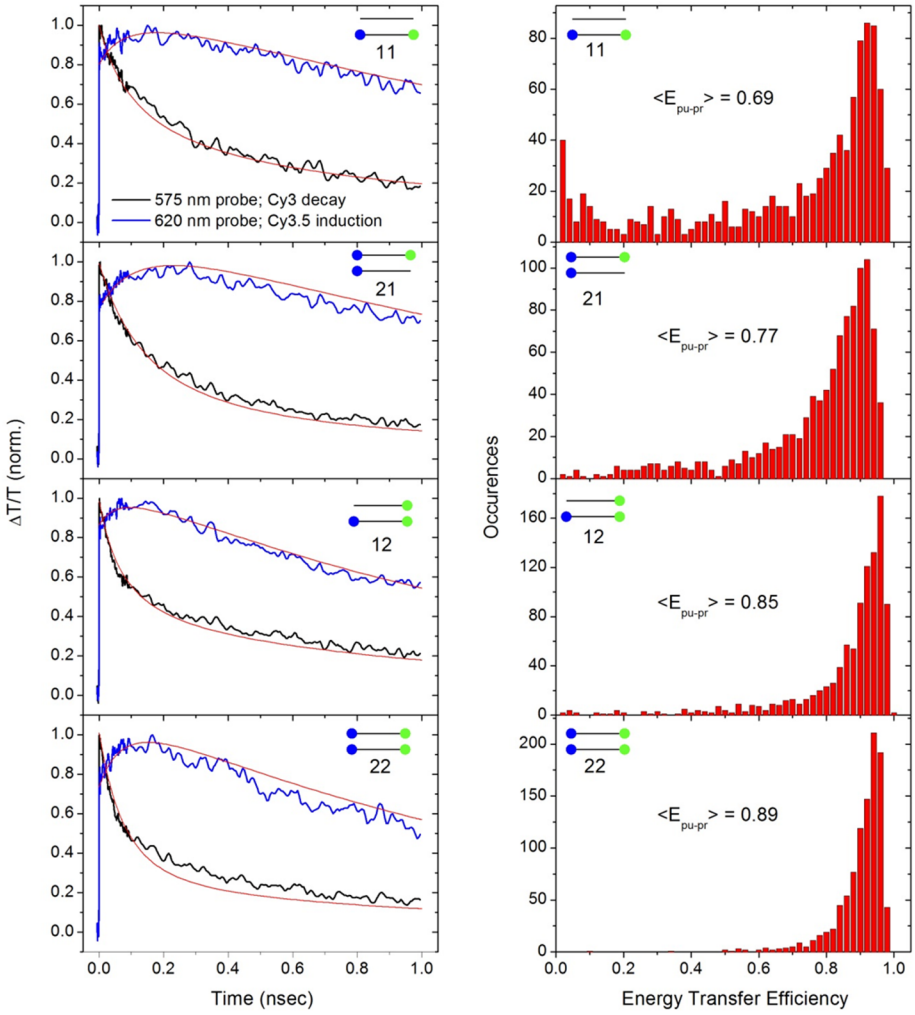

Figure 5. (Left) Donor decay and acceptor rise curves from ultrafast pump probe measurements (black and blue curves, respectively), and simulation of experimental results (red lines using the isotropic static distribution of κ^2). (Right) Histograms of energy transfer efficiency corresponding to the simulation results of the experimental ultrafast dynamics measurements. Histogram workup is described in the text. The average energy transfer efficiency is given in each panel.

case of **11**, the distribution is bimodal, with a broad peak containing the greater population fraction centered at a high efficiency of $E \sim 0.9$, and a second peak containing the lesser population fraction centered at low efficiency near $E \sim 0$. The broad tail that extends to the low efficiency side of the peak at $E \sim 0.9$ as well as the occurrence of the low FRET peak are due to the relative high probability of unfavorable transition dipoles. However, the distribution remains biased toward high FRET because of the relatively short separation ($r \sim 0.7\,\hat{R}_0$, using $r = 41$ Å obtained from the simulation) between Cy3 and Cy3.5. Addition of the second donor to make **21** opens a homo-FRET channel leading to a reduction of the low FRET population. Homo-FRET between donors provides two pathways for energy transfer to the acceptor, and thus increases the probability of finding a more favorable dipole orientation with respect to the acceptor. Without homo-FRET between donors, there is no increase in efficiency by adding a second donor. Adding instead a second acceptor to make **12** suppresses the occurrence of low FRET by opening an energy transfer pathway to a second acceptor. This also shifts the high FRET peak to slightly higher efficiency as a result of increasing the final states, which, in turn, increases the rate of energy transfer out of the donor. Finally, having both a second donor and a second acceptor (**22**) narrows the distribution and further shifts it to higher efficiency values due to the presence of both homo-FRET and the presence of two pathways from each donor to an acceptor. The average FRET efficiencies derived from the Monte Carlo simulation are also shown in Figure 5 (these are represented by $E_{\text{pu-pr}}$ because they are derived from the ultrafast pump−probe experiment). The values of $E_{\text{pu-pr}}$ are somewhat higher than those found from the steady state and time-resolved fluorescence measurements; however, the trend in $E_{\text{pu-pr}}$ is consistent with the prior measurements.

The simulations shown in Figure 6 more generally explore the potential benefits from having multiple donors and acceptors. The FRET efficiency is calculated versus the normalized separation distance $r/\hat{R}_0$ for both the dynamic limit, where $\kappa^2 = 2/3$, and static limits where the ensemble average is computed over an isotropic distribution of angles that yield the distribution of κ^2 in Figure S6. In the dynamic limit, the addition of a second donor (**21**) has no effect at any separation. Here, homo-FRET provides no benefit because all pathways result in the same efficiency. The addition of a second acceptor (**12**) improves the efficiency due to an increase in final states, which leads to an increase in the rate of energy transfer out of the donor. The relative increase in efficiency with respect to a single acceptor

DOI: 10.1021/acsphotonics.6b00006
ACS Photonics 2016, 3, 659−669

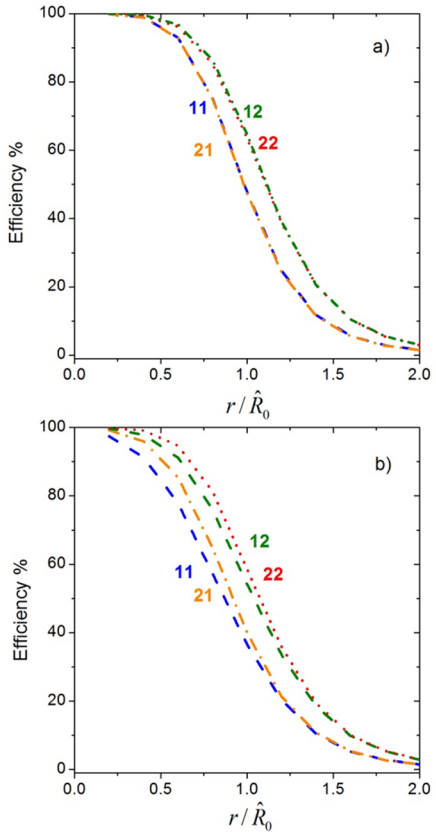

Figure 6. Simulation of energy transfer efficiency for dual rail constructs in (a) the dynamic and (b) static limits for the orientation factor κ^2. The simulations are calculated vs the normalized separation distance $r/\hat{R}_0$.

increases with $r/\hat{R}_0$ and asymptotically approaches a doubling of the relative efficiency (Figure S7). In the static limit, the addition of a second donor can modestly improve the efficiency beyond that of a single donor over a limited range of $r/\hat{R}_0$. From Figure 6, the relative increase in efficiency from a second donor peaks at about 13% at $r/\hat{R}_0 \sim 0.8$ (see also Figure S7). For $r/\hat{R}_0 > 1.5$, the benefit from homo-FRET becomes negligible because finding a significantly more efficient pathway becomes increasingly unlikely at larger separations. Similar to the case of dynamic averaging, the addition of a second acceptor improves the FRET efficiency at all separations (within the Förster theory limit) with the relative increase approaching a factor of 2 at large separations ($r/\hat{R}_0 > 1.5$) and reflecting the doubling of final states. The benefit in efficiency diminishes at closer separations because the relative cost of the extra homo-FRET step rises (Figure S7). Consistent with the experimental results, the highest efficiencies from the model are found to occur for the case of **22**.

It is useful to summarize the size of the experimental increases in FRET efficiency and compare them to those predicted by theory in the static isotropic limit (Figure 6). To do this, we average the FRET efficiencies determined by the three measurement methods in Table 1. Thus, adding a second donor to single acceptor (**11** → **21**) results in a 10% increase in FRET efficiency; adding a second acceptor to a single donor (**11** → **12**) results in a 19% in increase in FRET efficiency; adding both a second donor and second acceptor (**11** → **22**) results in 27% increase in FRET efficiency. The corresponding increases predicted by theory (using $r/R_0 = 0.7$ from the Monte Carlo modeling) are 12% (**11** → **21**), 23% (**11** → **12**), and 29% (**11** → **22**). While the experimental increases in the FRET efficiency are all somewhat lower than those predicted by theory, there is agreement in trend. One possible reason for the quantitative discrepancy is that a fully isotropic distribution of static transition dipoles may not be achieved in the sample.

It is also important to address the observation that the time-resolved measurements (E_{TR} and $E_{pu\text{-}pr}$) show larger increases in energy transfer efficiency upon adding a second donor than do the steady state measurements (E_{sens}, E_{DL}). Comparing **11** and **21** from Table 1 and Figure 5, the increase in efficiency for E_{TR} ($E_{pu\text{-}pr}$) is ∼16% (12%), while it is ∼10% for E_{sens} and ∼4% for E_{DL}. Similarly, comparing **12** and **22**, the increase in efficiency for E_{TR} ($E_{pu\text{-}pr}$) is ∼11% (5%), while it is ∼7% for E_{sens} and 4% for E_{DL}. This discrepancy is difficult to fully explain. One possibility is that there is some error in the concentration and quantum yields of the control and target structures that are needed to determine FRET efficiency from E_{DL} and E_{sens}. In contrast, the time-resolved methods do not require precise knowledge of fluorophore quantum yields and concentration of FRET and control structures. A second possibility may be due to incomplete formation of the target structures, where the steady-state and time-resolved methods may have different sensitivity to defect structures present in the ensemble. As one example, if the defect **x2** exists within the target **22** population then this would tend to decrease the efficiency measured by the steady state methods but not the observed induction rate of the acceptor. Nevertheless, the different measurements of FRET are consistent in that the efficiency increases in the order **11** < **21** < **12** < **22** in each case.

We comment on the relationship of our work to a previous work[45] that explored the effect of multiple donors and acceptors on FRET efficiency. Reference 45 studied protein samples conjugated with multiple donor dyes and multiple acceptor dyes. The number of donor dyes and acceptors dyes varied between one and five (for each donor and acceptor), covering all combinations between 1:1 and 5:5 (donor/acceptor). Perhaps somewhat surprisingly, a significant increase in FRET efficiency due to homo-FRET was observed only for the case of five donor dyes coupled to between one and five acceptor dyes; fewer donor dyes coupled to the same number of acceptors produced little, if any, increase in FRET efficiency. Our observation of increased efficiency from homo-FRET (∼10%: **11** → **21**) appears to be consistent with the magnitude of the increased FRET efficiency (∼10−20%) observed in ref 45. However, a meaningful comparison with that work is difficult because the geometrical arrangement of the dyes and interdye distances were not specified nor was it clear what the time scale of dye reorientation was (i.e., dynamic vs static limit), thus, making it difficult to fully understand the role of homo-FRET. In our work, a deeper understanding of the effect of homo-FRET is possible. This is because our structures enable the demonstration of increased energy transfer from homo-FRET in the simplest case of two donors coupled to a single acceptor, a more precise knowledge of interfluorophore geometrical arrangement and distances is available, and we have experimentally demonstrated the limit of static fluorophores.

CONCLUSIONS

In summary, we have investigated the FRET properties for a system consisting of two donor and two acceptor fluorophores linked to a rigid dual rail DNA scaffold. The close spacing of the fluorophores produces both homo-FRET and hetero-FRET interactions and results in multiple pathways from donor to

DOI: 10.1021/acsphotonics.6b00006
ACS Photonics 2016, 3, 659−669

acceptor fluorophores. We have shown experimentally and confirmed theoretically within the Förster picture that the multiple FRET pathways lead to an improvement in energy transfer efficiency with respect to a single pathway, where the donor and acceptor separation is unchanged. When the distribution of fluorophore orientations is static then homo-FRET between the donors opens an additional pathway, which improves the efficiency. For **11** → **21** and **12** → **22**, the improvements in FRET efficiency were ∼10% and ∼7%, respectively. The improvement is larger for the addition of the second acceptor, which not only has two paths to an acceptor, but also doubles the final states and, therefore, increases the rate of energy transfer out of the donor. For **11** → **12** and **21** → **22**, the improvements in FRET efficiency were ∼19% and ∼15%, respectively. Adding both a second donor and second acceptor (**11** → **22**) resulted in a 27% improvement in FRET efficiency. We note that for homo-FRET to provide an enhancement in efficiency, the rate of transfer between donors must be faster than both the inverse excited state lifetime and hetero-FRET rate. The ∼1 ps^{-1} homo-FRET rate observed from our DNA structures satisfies this condition. The benefits of multiple pathways could further improve energy transfer efficiency in larger FRET networks, as long as two conditions are maintained. First, the donor−acceptor distance should remain approximately constant. Within the static limit, if the donor−acceptor separation distance remains constant then additional donors will increase the efficiency, which will asymptotically approach the value for the dynamic limit. Second, the structure should be designed so that the increased complexity does not introduce significant competing nonradiative relaxation that returns electronic excitations to the molecular ground state before reaching the terminus of the FRET network. In particular, further benefits gained from homo-FRET will require optimization of the distance between donor fluorophores as to achieve sufficient homo-FRET rates without introducing self-quenching. A natural extension of this study would be to increase the number of pathways in the dual rail by increasing the steps of the FRET cascade. This could be done by inserting fluorophores with smaller S_0−S_1 transitions at the 3′ and 5′ ends of the unlabeled oligos (colored blue and yellow) in the dual rail structure shown in Figure 1a. Finally, multiple pathways can be effective in compensating for nonideal ensemble characteristics such as random static dipole orientation, and possibly even formation errors such as missing (or nonperforming) fluorophores.[5] Large DNA FRET networks such as those studied in refs 5 and 13 can be particularly susceptible to nonideal ensemble effects, thus, engineering multiple pathways into such FRET networks is an important design consideration for the goal of creating efficient synthetic light harvesting systems.

■ ASSOCIATED CONTENT

Supporting Information

The Supporting Information is available free of charge on the ACS Publications website at DOI: 10.1021/acsphotonics.6b00006.

DNA oligo sequences; fluorophore structures and linkers; electrophoresis results; steady-state spectra and time-resolved fluorescence of control structures; tables of optical and photophysical properties; homo-FRET measurement of donor-only control; and methodology used in the theoretical modeling of FRET dynamics (PDF).

■ AUTHOR INFORMATION

Corresponding Author

*E-mail: joseph.melinger@nrl.navy.mil.

Notes

The authors declare no competing financial interest.

■ ACKNOWLEDGMENTS

This work was supported by the Nanoscience Institute at the Naval Research Laboratory and the Office of Naval Research.

■ REFERENCES

(1) Rothemund, P. W. K. Folding DNA to create nanoscale shapes and patterns. *Nature* **2006**, *440*, 297−302.

(2) Pinheiro, A. V.; Han, D.; Shih, W. M.; Yan, H. Challenges and opportunities for structural DNA nanotechnology. *Nat. Nanotechnol.* **2011**, *6*, 763−772.

(3) Seeman, N. C. An overview of structural DNA Nanotechnology. *Mol. Biotechnol.* **2007**, *37*, 246−257.

(4) He, Y.; Ye, T.; Su, M.; Zhang, C.; Ribbe, A. E.; Jiang, W.; Mao, C. D. Hierarchical self-assembly of DNA into symmetric supramolecular polyhedra. *Nature* **2008**, *452*, 198−U41.

(5) Buckhout-White, S.; Spillmann, C. M.; Algar, W. R.; Khachatrian, A.; Melinger, J. S.; Goldman, E. R.; Ancona, M. G.; Medintz, I. L. Assembling programmable FRET-based photonic networks using designer DNA scaffolds. *Nat. Commun.* **2014**, *5*, 1−16.

(6) Cunningham, P. D.; Khachatrian, A.; Buckhout-White, S.; Deschamps, J. R.; Goldman, E. R.; Medintz, I. L.; Melinger, J. S. Resonance Energy Transfer in DNA Duplexes Labeled with Localized Dyes. *J. Phys. Chem. B* **2014**, *118*, 14555−14565.

(7) Buckhout-White, S.; Claussen, J. C.; Melinger, J. S.; Dunningham, Z.; Ancona, M. G.; Goldman, E. R.; Medintz, I. L. A triangular three-dye DNA switch capable of reconfigurable molecular logic. *RSC Adv.* **2014**, *4*, 48860−48871.

(8) Wang, F.; Lu, C. H.; Willner, I. From Cascaded Catalytic Nucleic Acids to Enzyme-DNA Nanostructures: Controlling Reactivity, Sensing, Logic Operations, and Assembly of Complex Structures. *Chem. Rev.* **2014**, *114*, 2881−2941.

(9) Elbaz, J.; Lioubashevski, O.; Wang, F.; Remacle, F.; Levine, R. D.; Willner, I. DNA computing circuits using libraries of DNAzyme subunits. *Nat. Nanotechnol.* **2010**, *5*, 417−422.

(10) Mottaghi, M. D.; Dwyer, C. Thousand-Fold Increase in Optical Storage Density by Polychromatic Address Multiplexing on Self-Assembled DNA Nanostructures. *Adv. Mater.* **2013**, *25*, 3593−3598.

(11) Samain, F.; Ghosh, S.; Teo, Y. N.; Kool, E. T. Polyfluorophores on a DNA Backbone: Sensors of Small Molecules in the Vapor Phase. *Angew. Chem., Int. Ed.* **2010**, *49*, 7025−7029.

(12) Teo, Y. N.; Kool, E. T. DNA-Multichromophore Systems. *Chem. Rev.* **2012**, *112*, 4221−4245.

(13) Modi, S.; Nizak, C.; Surana, S.; Halder, S.; Krishnan, Y. Two DNA nanomachines map pH changes along intersecting endocytic pathways inside the same cell. *Nat. Nanotechnol.* **2013**, *8*, 459−467.

(14) Pei, H.; Zuo, X.; Pan, D.; Shi, J.; Huang, Q.; Fan, C. Scaffolded biosensors with designed DNA nanostructures. *NPG Asia Mater.* **2013**, *5*, e51.

(15) Dutta, P. K.; Varghese, R.; Nangreave, J.; Lin, S.; Yan, H.; Liu, Y. DNA-Directed Artificial Light-Harvesting Antenna. *J. Am. Chem. Soc.* **2011**, *133*, 11985−11993.

(16) Albinsson, B.; Hannestad, J. K.; Borjesson, K. Functionalized DNA nanostructures for light harvesting and charge separation. *Coord. Chem. Rev.* **2012**, *256*, 2399−2413.

(17) Lewis, F. D.; Zhang, L.; Zuo, X. Orientation Control of Fluorescence Resonance Energy Transfer Using DNA as a Helical Scaffold. *J. Am. Chem. Soc.* **2005**, *127*, 10002−10003.

(18) Iqbal, A.; Arslan, S.; Okumus, B.; Wilson, T. J.; Giraud, G.; Norman, D. G.; Ha, T.; Lilley, D. M. J. Orientation dependence in fluorescent energy transfer between Cy3 and Cy5 terminally attached to

DOI: 10.1021/acsphotonics.6b00006
ACS Photonics 2016, 3, 659−669

double-stranded nucleic acids. *Proc. Natl. Acad. Sci. U. S. A.* **2008**, *105*, 11176−11181.
(19) Kato, T.; Kashida, H.; Kishida, H.; Yada, H.; Okamoto, H.; Asanuma, H. Development of a Robust Model System of FRET using Base Surrogates Tethering Fluorophores for Strict Control of Their Position and Orientation within DNA Duplex. *J. Am. Chem. Soc.* **2013**, *135*, 741−750.
(20) Dietrich, A.; Buschmann, V.; Müller, C.; Sauer, M. Fluorescence resonance energy transfer (FRET) and competing processes in donor-acceptor substituted DNA strands: a comparative study of ensemble and single-molecule data. *Rev. Mol. Biotechnol.* **2002**, *82*, 211−231.
(21) Sindbert, S.; Kalinin, S.; Nguyen, H.; Kienzler, A.; Clima, L.; Bannwarth, W.; Appel, B.; Muller, S.; Seidel, C. A. M. Accurate Distance Determination of Nucleic Acids via Forster Resonance Energy Transfer: Implications of Dye Linker Length and Rigidity. *J. Am. Chem. Soc.* **2011**, *133*, 2463−2480.
(22) Vogel, S. S.; van der Meer, B. W.; Blank, P. S. Estimating the distance separating fluorescent protein FRET pairs. *Methods* **2014**, *66*, 131−138.
(23) van Grondelle, R.; Novoderezhkin, V. I. Energy transfer in photosynthesis: experimental insights and quantitative models. *Phys. Chem. Chem. Phys.* **2006**, *8*, 793−807.
(24) Adronov, A.; Gilat, S. L.; Frechet, J. M. J.; Ohta, K.; Neuwahl, F. V. R.; Fleming, G. R. Light Harvesting and Energy Transfer in Laser Dye-Labeled Poly(aryl ether) Dendrimers. *J. Am. Chem. Soc.* **2000**, *122*, 1175−1185.
(25) Devadoss, C.; Bharathi, P.; Moore, J. S. Energy Transfer in Dendritic Macromolecules: Molecular Size Effects and the Role of an Energy Gradient. *J. Am. Chem. Soc.* **1996**, *118*, 9635−9644.
(26) Melinger, J. S.; Pan, Y.; Kleiman, V. D.; Peng, Z.; Davis, B. L.; McMorrow, D.; Lu, M. Optical and Photophysical Properties of Light-Harvesting Phenylacetylene Monodendrons Based on Unsymmetrical Branching. *J. Am. Chem. Soc.* **2002**, *124*, 12002−12012.
(27) Winfree, E.; Liu, F.; Wenzler, L. A.; Seeman, N. C. Design and self-assembly of two-dimensional DNA crystals. *Nature* **1998**, *394*, 539−544.
(28) Spillmann, C. M.; Ancona, M. G.; Buckhout-White, S.; Algar, W. R.; Stewart, M. H.; Susumu, K.; Huston, A. L.; Goldman, E. R.; Medintz, I. L. Achieving Effective Terminal Exciton Delivery in Quantum Dot Antenna-Sensitized Multistep DNA Photonic Wires. *ACS Nano* **2013**, *7*, 7101−7118.
(29) Arbeloa, F. L. p.; Ojeda, P. R.; Arbeloa, I. L. p. Flourescence self-quenching of the molecular forms of Rhodamine B in aqueous and ethanolic solutions. *J. Lumin.* **1989**, *44*, 105−112.
(30) Birge, R. R. Kodak Laser Dyes. *Kodak Publication JJ-169*; Kodak, 1987.
(31) Lakowicz, J. R. *Principles of Fluorescence Spectroscopy*, 2nd ed.; Kluwer Academic/Plenum Publishers: New York, 1999; p 369.
(32) Boeneman, K.; Prasuhn, D. E.; Blanco-Canosa, J. B.; Dawson, P. E.; Melinger, J. S.; Ancona, M.; Stewart, M. H.; Susumu, K.; Huston, A.; Medintz, I. L. Self-Assembled Quantum Dot-Sensitized Multivalent DNA Photonic Wires. *J. Am. Chem. Soc.* **2010**, *132*, 18177−18190.
(33) Hannestad, J. K.; Sandin, P.; Albinsson, B. Self-Assembled DNA Photonic Wire for Long-Range Energy Transfer. *J. Am. Chem. Soc.* **2008**, *130*, 15889−15895.
(34) Tao, T. Time-dependent fluorescence depolarization and Brownian rotational diffusion coefficients of macromolecules. *Biopolymers* **1969**, *8*, 609−632.
(35) Ranjit, S.; Gurunathan, K.; Levitus, M. Photophysics of Backbone Fluorescent DNA Modifications: Reducing Uncertainties in FRET. *J. Phys. Chem. B* **2009**, *113*, 7861−7866.
(36) Fu, T. J.; Seeman, N. C. *Biochemistry* **1993**, *32*, 3211.
(37) Johansson, M. K.; Fidder, H.; Dick, D.; Cook, R. M. Intramolecular Dimers: A New Strategy to Fluorescence Quenching in Dual-Labeled Oligonucleotide Probes. *J. Am. Chem. Soc.* **2002**, *124*, 6950−6956.
(38) Ramreddy, T.; Rao; Krishnamoorthy, G. Site-Specific Dynamics of Strands in ss- and dsDNA As Revealed by Time-Domain Fluorescence of 2-Aminopurine. *J. Phys. Chem. B* **2007**, *111*, 5757−5766.
(39) Sanborn, M. E.; Connolly, B. K.; Gurunathan, K.; Levitus, M. Fluorescence Properties and Photophysics of the Sulfoindocyanine Cy3 Linked Covalently to DNA. *J. Phys. Chem. B* **2007**, *111*, 11064−11074.
(40) Watrob, H. M.; Pan, C.-P.; Barkley, M. D. Two-Step FRET as a Structural Tool. *J. Am. Chem. Soc.* **2003**, *125*, 7336−7343.
(41) Berberan-Santos, M. N.; Valeur, B. Fluorescence depolarization by electronic energy transfer in donor-acceptor pairs of like and unlike chromophores. *J. Chem. Phys.* **1991**, *95*, 8048−8055.
(42) Fei, J.; Ha, T. Watching DNA breathe one molecule at a time. *Proc. Natl. Acad. Sci. U. S. A.* **2013**, *110*, 17173−17174.
(43) Hinze, G.; Métivier, R.; Nolde, F.; Müllen, K.; Bäsche, T. Intramolecular electronic excitation energy transfer in donor-acceptor dyads studied by time and frequency resolved single molecule spectroscopy. *J. Chem. Phys.* **2008**, *128*, 124516.
(44) Munoz-Losa, A.; Curutchet, C.; Krueger, B. P.; Hartsell, L. R.; Mennucci, B. Fretting about FRET: Failure of the Ideal Dipole Approximation. *Biophys. J.* **2009**, *96*, 4779−4788.
(45) Fábián, Á. I.; Rente, T.; Szöllősi, J.; Mátyus, L.; Jenei, A. Strength in Numbers: Effects of Acceptor Abundance on FRET Efficiency. *ChemPhysChem* **2010**, *11*, 3713−3721.

DOI: 10.1021/acsphotonics.6b00006
ACS Photonics 2016, 3, 659−669